BBA - Molecular Basis of Disease 1866 (2020) 165742

Contents lists available at ScienceDirect

BBA - Molecular Basis of Disease

journal homepage: www.elsevier.com/locate/bbadis

Insights into the molecular pathogenesis of cardiospondylocarpofacial syndrome: *MAP3K7* c.737-7A > G variant alters the TGFβ-mediated α-SMA cytoskeleton assembly and autophagy

Lucia Micale[a,*], Silvia Morlino[b], Tommaso Biagini[c], Annalucia Carbone[d], Carmela Fusco[a], Marco Ritelli[e], Vincenzo Giambra[f], Nicoletta Zoppi[e], Grazia Nardella[a,g], Angelantonio Notarangelo[a], Annalisa Schirizzi[a,h], Gianluigi Mazzoccoli[d], Paola Grammatico[b], Emma M. Wade[i], Tommaso Mazza[c], Marina Colombi[e], Marco Castori[a]

[a] Division of Medical Genetics, Fondazione IRCCS Casa Sollievo della Sofferenza, San Giovanni Rotondo, Foggia, Italy
[b] Laboratory of Medical Genetics, Department of Molecular Medicine, Sapienza University, San Camillo-Forlanini Hospital, Rome, Italy
[c] Unit of Bioinformatics, Fondazione IRCCS Casa Sollievo della Sofferenza, San Giovanni Rotondo, Foggia, Italy
[d] Division of Internal Medicine and Unit of Chronobiology, Fondazione IRCCS Casa Sollievo della Sofferenza, San Giovanni Rotondo, Foggia, Italy
[e] Division of Biology and Genetics, Department of Molecular and Translational Medicine, University of Brescia, Brescia, Italy
[f] Institute for Stem Cell Biology, Regenerative Medicine and Innovative Therapies (ISBReMIT), Fondazione IRCCS Casa Sollievo della Sofferenza, San Giovanni Rotondo, Foggia, Italy
[g] Department of Experimental Medicine, Sapienza University of Rome, Rome, Italy
[h] Dipartimento di Biologia, Università degli Studi di Bari, "Aldo Moro", Bari, Italy
[i] Department of Women's and Children's Health, Dunedin School of Medicine, University of Otago, Dunedin, New Zealand

ARTICLE INFO

Keywords:
Cardiospondylocarpofacial syndrome
Connective tissue
TAB1
TAK1
α-SMA cytoskeleton
TGFβ

ABSTRACT

Transforming growth factor beta-activated kinase 1 (TAK1) is a highly conserved kinase protein encoded by *MAP3K7,* and activated by multiple extracellular stimuli, growth factors and cytokines. Heterozygous variants in *MAP3K7* cause the cardiospondylocarpofacial syndrome (CSCFS) which is characterized by short stature, dysmorphic facial features, cardiac septal defects with valve dysplasia, and skeletal anomalies. CSCFS has been described in seven patients to date and its molecular pathogenesis is only partially understood. Here, the functional effects of the *MAP3K7 c.737-7A > G* variant, previously identified in a girl with CSCFS and additional soft connective tissue features, were explored. This splice variant generates an in-frame insertion of 2 amino acid residues in the kinase domain of TAK1. Computational analysis revealed that this in-frame insertion alters protein dynamics in the kinase activation loop responsible for TAK1 autophosphorylation after binding with its interactor TAB1. Co-immunoprecipitation studies demonstrate that the ectopic expression of TAK1-mutated protein impairs its ability to physically bind TAB1. In patient's fibroblasts, *MAP3K7 c.737-7A > G* variant results in reduced TAK1 autophosphorylation and dysregulation of the downstream TAK1-dependent signaling pathway. TAK1 loss-of-function is associated with an impaired TGFβ-mediated α-SMA cytoskeleton assembly and cell migration, and defective autophagy process. These findings contribute to our understanding of the molecular pathogenesis of CSCFS and might offer the rationale for the design of novel therapeutic targets.

Abbreviations: FBN, fibrillin; CHX, cycloheximide; COLL, collagens; CSCFS, cardiospondylocarpofacial syndrome; D-MEM, Dulbecco's-Modified Eagle Medium; ECM, extracellular matrix; HEK, human embryonic kidney; FMD2, frontometaphyseal dysplasia type 2; FN, fibronectin; IL-1, interleukin-1; MAPK-SRE, MAPK-responsive element; MD, molecular dynamic; NF-κB, Nuclear factor κ-B; NF-kB-RE, NF-kB responsive elements; NS, nanoseconds; PBS, phosphate buffered saline; PTMs, post-translational modifications; RMSD, root-mean-square deviation; RMSF, root-mean-square fluctuation; SDS-PAGE, sulphate - polyacrylamide gel electrophoresis; TAK1, transforming growth factor beta-activated kinase 1; TNFα, tumor necrosis factors α; αSMA, α-smooth muscle actin

* Corresponding author at: Division of Medical Genetics, Fondazione IRCCS Casa Sollievo della Sofferenza, Poliambulatorio "Papa Giovanni Paolo II", 2nd Floor, Viale Padre Pio, 7, 71013 San Giovanni Rotondo, FG, Italy.
E-mail address: l.micale@operapadrepio.it (L. Micale).

https://doi.org/10.1016/j.bbadis.2020.165742
Received 9 January 2020; Received in revised form 20 February 2020; Accepted 21 February 2020
Available online 24 February 2020
0925-4439/

1. Introduction

Transforming growth factor β (TGFβ) activated kinase 1 (TAK1) is a serine/threonine kinase belonging to the MAP3K family and is encoded by *MAP3K7*, which maps to 6q15. TAK1 orchestrates inflammatory response and cell survival through the integration of different extracellular signaling networks, including TGF-β, interleukin-1 (IL-1), tumor necrosis factors α (TNFα), and Toll-like receptors pathways [1] Nuclear factor κ-B (NF-κB) and activated protein-1 are the main downstream effectors of TAK1 and are activated by specific extracellular stimuli [2]. TAK1 kinase activity is strictly regulated by multiple post-translational modifications (PTMs), such as phosphorylation/dephosphorylation and ubiquitination. These stimuli and cell-type dependent PTMs reflect the complexity of TAK1-dependent signaling and are modulated by TAK1 itself and several associated proteins. Among them, TAK1 binding proteins (TABs) are required to regulate TAK1 activity. TAK1 is constitutively coupled with TAB1 and binds TAB2 or TAB3 after stimulation [3]. In particular, TAB1 contains C-terminal and N-terminal pseudo-phosphatase domains, which are necessary to bind and activate TAK1 [4]. Studies in embryonic fibroblasts from *Tab1*-deficient mice demonstrate that TAB1 is essential for TAK1 activity and TGFβ signal transduction [5]. On the other hand, TAB2 or TAB3 act as scaffold proteins and promote the interaction of TAK1/TAB1 complex to TRAF6 protein [3].

Accumulating evidences reveal that TGFβ1-induced TAK1 signaling plays a critical role in extracellular matrix (ECM) homeostasis and in mediating fibrotic response. The ECM is a complex mixture of carbohydrates and proteins that includes collagens, proteoglycans, and glycoproteins [6], which are the principal components of the connective tissue and their abnormalities are associated to a wide range of hereditary connective tissue disorders. TAK1 is a major upstream signaling molecule mediating TGFβ1-induced expression of type I and IV collagens (COLL) and fibronectin (FN) in cultured primary mesangial cells [7–9]. In addition, TAK1 deficiency exhibits a reduced profibrotic response to TGFβ1 stimulation in mice fibroblasts [10]. ECM deposition and profibrotic response can be also influenced by other TGFβ-mediated pathways cross-talking with the TAK1 signaling [11,12].

Analysis of conditional knockout mice reveals that *Map3k7* deficiency causes various types of defects, such as abnormal cell differentiation, increased cell death and decreased inflammatory responses due to impaired Tak1 signaling [2]. In human, abnormalities of TAK1 signaling are associated with a variety of acquired disorders, such as renal inflammation and fibrosis [13], contact hypersensitivity response [14], neuronal death in cerebral ischemia [15], autoimmune diseases, and cancer [2]. Specific germline *MAP3K7* heterozygous variants are related to the ultrarare cardiospondylocarpofacial syndrome (CSCFS, OMIM #157800) [16,17] which is characterized by growth retardation, dysmorphic facial features, cardiac septal defects with valve dysplasia, conductive deafness, and skeletal anomalies. Heterozygous alleles in *MAP3K7* also cause the frontometaphyseal dysplasia type 2 (FMD2, OMIM #617137) [16,17]. These two disorders do not overlap suggesting different mechanisms underlying their pathogenesis. However, the limited available functional data together with the small number of reported patients do not completely explain such a heterogeneity.

Recently, we described a CSCFS patient with multiple additional soft connective tissue features and carrying the novel *MAP3K7* c.737-7A > G variant [18]. In the present work, we widely explored the functional effects of this *MAP3K7* splicing variant in order to explain the associated multisystem phenotype. Functional studies demonstrated that the expression of TAK1-mutated protein impairs its ability to physically bind TAB1. In patient's fibroblasts, *MAP3K7 c.737-7A > G* variant results in an altered intracellular TAK1-dependent signaling which causes a broad-spectrum of clinical features displayed by our CSCFS individual.

2. Materials and methods

2.1. Patient and samples

This study focused on the *MAP3K7* (RefSeq NM_145331) c.737-7A > G variant previously identified in a patient with CSCFS [19]. This variant has been submitted to the LOVD (Leiden Open Variation Database, https://databases.lovd.nl/shared/variants/0000222104, individual ID #00132079). Briefly, the patient was a 6 and 6/12-year-old girl with facial dysmorphism, heart valve dysplasia, mild hypoplasia of the aortic arch, short stature, severe gastroesophageal reflux, generalized joint hypermobility, soft and velvety skin, multiple vertebral fusions, transmission deafness [19]. The combination of the CSCFS key features, and the articular and skin findings was previously unreported. She and her unaffected parents underwent blood sampling and skin biopsy for the following investigations, and approved publication after signing the informed consent. This study is in accordance with the 1984 Helsinki declaration and its following modifications, and conservation and use of biological samples for scientific purposes were approved by the local ethics committee (protocol no. GTB12001).

2.2. Conservation of TAK1 (Asn245) amino acid

Evolutionary conservation of the TAK1 region including Asn245 and Gly246 amino acids was explored with protein sequence alignment generated by Clustal Omega (https://www.ebi.ac.uk/Tools/msa/clustalo/) and compared with data provided by UCSC Database (https://genome.ucsc.edu).

2.3. Molecular dynamics simulation

Atomic coordinates of TAK1 were obtained from the Protein Data Bank (PDB id: 2EVA) and used for molecular dynamics (MD) simulations as described in [20]. The wild-type model was mutated *in silico* (Asn245_Gly246insValVal) through UCSC Chimera. The resulting two models, indicated as the wild-type (wt) and mutated models, were embedded in boxes, extending up to 12 Å, and solvated using the TIP3P water model. The *tleap* tool was used to add counter ions and thus to neutralize the overall charge of the models. Each model was first energy minimized and then equilibrated for approximately 5 ns, by time steps of 1 fs. MD simulations were performed three times on the three equilibrated models for 360 ns by time steps of 2 fs, namely for 100 million steps. A 10 Å cutoff was used for non-bonded short-range interactions and long-range electrostatics were treated with the particle-mesh Ewald method. Temperature and pressure were maintained at 300 K and 101.3 kPa, respectively, using the Langevin dynamics and piston method. The Gromacs tools *g_rms, g_rmsf* and *do_dssp* were used to calculate the (i) root-mean-square deviation (RMSD), which measures the average distance between all heavy atoms (C_α atomic coordinates in this case) with respect to the X-ray structure; (ii) per-residue root-mean-square fluctuation (RMSF), which measures the deviation over time of the positions of the C_α atomic coordinates of each residue with respect to the X-ray structure; and (iii) secondary structure content and dynamic cross-correlation maps (DCCMs), which allow to investigate the long-range interactions of atoms. Colors of the C_{ij} elements of the map were indicative of strong to moderate positive correlated (red to green) or of strong to moderate anti-correlated (dark to light blue) motion of residues *i* and *j*. Each of these indices was calculated for both the wt and mutant proteins.

2.4. Cell cultures

Primary dermal fibroblasts were established from skin biopsies of the patient and her parents (as the variant occurred "*de novo*" without evidence of somatic mosaicism, these two individuals were used as internal controls) and cultured in Dulbecco's-Modified Eagle Medium/

Nutrient Mixture F-12 (D-MEMF12) (Thermo Fisher Scientific, USA) plus 20% fetal bovine serum (FBS) (Thermo Fisher Scientific, USA) and 1% penicillin and streptomycin (P/S, 100 U/ml and 100 μg/ml, respectively) (Thermo Fisher Scientific, USA). Primary fibroblast cultures were deposited into the Genomic and Genetic Disorders Biobank (GGDB, http://www.operapadrepio.it/ggdbbank/). Human embryonic kidney (HEK) 293 cell lines were maintained in D-MEM with Glutamax supplemented with 10% FBS and 1% P/S. Cell cultures were grown in a 5% CO_2 incubator at 37 °C.

2.5. RNA extraction and reverse transcription

Total RNA was extracted with the RNeasy Mini Kit (Qiagen, Germany), treated with RNase free-DNase- (Qiagen, Germany), quantified by Nanodrop (Thermo Fisher Scientific, USA), and reverse-transcribed with the QuantiTect Reverse Transcription Kit (Qiagen, Germany), according to the manufacturer's protocol. cDNA amplification and Sanger sequencing were carried out with primers listed in Table S1.

2.6. Generation of expression plasmid

The pcDNA3 construct expressing the FLAG-tagged-p.(Asn245_Gly246insValVal) TAK1 variant was generated from FLAG-tagged-TAK1 wt by using the QuickChange II site-directed mutagenesis kit (Stratagene, USA) and a Pfu Taq polymerase (Promega, USA), according to the manufacturer's instructions. The construct was verified by Sanger sequencing. Primer pairs used are listed in Table S1.

2.7. Co-immunoprecipitation assay and Western blot

HEK293 cells were plated in 100 mm culture dishes at a density of 5×10^5 cells/ml and then transfected with FLAG-tagged wt or FLAG-tagged-p.(Asn245_Gly246insValVal) TAK1 plasmids or FLAG-empty vector by using Lipofectamine® LTX (Thermo Fisher Scientific, USA), according to manufacturer's instructions. After 48 h, cells were lysed in RIPA buffer and co-immunoprecipitated with anti-FLAG (#F3165, Sigma Aldrich, Germany) using Dynabeads magnetic beads (Thermo Fisher Scientific, USA). Immuno-complexes were resolved by 10% sodium dodecyl sulphate - polyacrylamide gel electrophoresis (SDS-PAGE), followed by transfer to a nitrocellulose membrane. Membrane was blocked in gelatin (VWR International, USA) and immunoblotted with anti-FLAG and anti-TAB1 (# S828A 3° b, MRC PPU Reagent, UK) antibodies (Abs), as reported previously [38,39], followed by secondary horseradish peroxidase conjugated anti-mouse and anti-rabbit (Santa Cruz, USA) Abs, respectively. The detection of protein samples was carried out by using a chemiluminescence reaction (GE Healthcare, UK).

2.8. Protein stability analysis

HEK293 cells were plated in a 12-well dish at a density of 2.0×10^5 cells/ml and then transfected with FLAG-tagged-TAK1 wt or FLAG-tagged-p.(Asn245_Gly246insValVal) TAK1 plasmids by using Lipofectamine® LTX. After 24 h, cells were cultured with 85 μg/mL cycloheximide (CHX, #cay14126–1, Biomol, USA) or dimethyl sulphoxide (DMSO, #D2650, Sigma Aldrich, Germany) as control, as previously reported [21]. Transfections were harvested after 0, 4, 8, and 10 h of CHX treatment and then lysed in 1× phosphate buffered saline (PBS) and 0.025% NP-40 with protease inhibitors (Roche, USA). The supernatants were cleared by centrifugation and resolved by electrophoresis on 10% SDS-PAGE gel and subjected to immunoblotting with anti-FLAG and-GAPDH (#sc-47,724, Santa Cruz, USA) Abs.

2.9. Luciferase assay

HEK293 cells were seeded at density of 1.0×10^5 cells/ml per well in a 24-wells plate and then transfected with pGL4.32-NF-kB-RE (E849A, Promega, USA) or (pGL4.33-MAPK-SRE (E134A, Promega, Madison, WI, USA) luciferase reporter plasmid together with indicated expression vector using Lipofectamine® LTX (Thermo Fisher Scientific, USA), according to manufacturer's instructions. *Renilla* luciferase-expressing plasmid (pRL-SV40, Promega, USA) was used to normalize transfection efficiencies. 48 h after transfection, cells were lysed in the passive buffer and assayed for both firefly and *Renilla* luciferase activities using the Dual-GLO® Luciferase Assay System (Promega, USA) in a Glomax 96 microplate luminometer (Promega, USA). Firefly luciferase activity was normalized to *Renilla* luciferase activity for each transfected well. Values are the mean ± SEM of three experimental replicates from three independent transfections.

2.10. Quantification of phosphorylated protein level

Patient's and controls' fibroblasts were lysed in 1× D-PBS, 0.025% NP-40, and protease- and phospho-inhibitors (Roche, USA), resolved by electrophoresis on 10% SDS-PAGE, and transferred to nitrocellulose membrane. Membranes were blocked in gelatin and then blotted with the following Abs: anti-MAPK (#4695, Cell Signaling, The Netherlands), anti-phospho-MAPK (#4370, Cell Signaling, The Netherlands), anti-NF-kB (#8242, Cell Signaling, The Netherlands), anti-TAK1 (#S828A, MRC PPU Reagent, UK), anti-phospho-TAK1 (#9339, Cell Signaling, The Netherlands), and anti-GAPDH (#sc-47,724, Santa Cruz, USA). To analyze the reactive MAPK or TAK1 phosphorylation level, bands intensity of phosphorylated (p)-MAPK/MAPK or (p)-TAK1/TAK1 was quantified using Image J software, as previously reported [22].

2.11. Immunofluorescence microscopy

To analyze the ECM organization of collagen type I (COLLI), type III (COLLIII), type V (COLLV), and FN, skin fibroblasts derived either from the patient or her unaffected mother and father, were grown for 72 h and immunoreacted as previously reported [23–25]. We used the following antibodies: (COLLI, #AB758, COLLIII, #AB758, COLLV, #AB781, Merke Millipore, USA and FN, #F3648, Sigma Aldrich, Germany), To analyze the ECM of fibrillins (FBNs), fibroblasts from the patient (Pt) and her unaffected mother and father were grown for 72 h, fixed in cold methanol and immunoreacted with 1 μg/ml anti-FBNs monoclonal Ab (#MS-231-P1-Clone 11C1.3) (NeoMarkers Fremont, CA, USA), which recognizes all FBN isoforms. To analyze the organization of the α-SMA cytoskeleton, fibroblasts grown to confluence were maintained for 12 h in serum-free medium supplemented or not with 10 ng/ml of TGFβ (#T1654, Sigma Aldrich, Germany), fixed in cold methanol, and immunoreacted for 1 h with 1 μg/ml anti-α-SMA monoclonal Ab (#A5228-Clone 1A) (Sigma Aldrich, Germany), as previously reported [26]. Cells were incubated for 1 h with Alexa Fluor 488 anti-rabbit and Alexa Fluor 594 anti-mouse Abs (Thermo Fisher Scientific, USA), or with rhodamine-conjugated anti-goat IgG (Calbiochem-Merck, Germany). Immunofluorescence signals were acquired by a black-and-white CCD TV camera (SensiCam-PCO Computer Optics GmbH, Germany) mounted on a Zeiss fluorescence Axiovert microscope and digitalized by Image Pro Plus software (Media Cybernetics, USA). The experiments were repeated three times. To analyze the localization and the signal intensity of endogenous LC3, fibroblasts were plated in 3 cm culture dishes and maintained for 4 h in complete or serum-free medium supplemented or not with 10 ng/ml of TGFβ. After treatments, cells were fixed in cold methanol, blocked in 1× PBS and 1% bovine serum albumin, and incubated with anti α-LC3 Ab (#NB100–2220, Novus, USA). After incubation with Alexa Fluor 568 anti-rabbit followed by DAPI (Thermo Fisher Scientific, USA) staining, cells were

covered with a drop of mounting medium and examined on a Leica TCS SP8 confocal microscopy (Leica, Wetzlar, Germany). All confocal images were obtained using the necessary filter sets for Alexa Fluor 568 and a x40 (1.2 numerical aperture) water immersion objective. Acquisition of data was performed with the same intensity settings and quantified measuring the relative intensity of pixels representative for each region of interest (ROI) corresponding of a single cell by eLAS X software (Leica, Wetzlar, Germany).

2.12. Migration assay

Cell migration was evaluated in a Transwell assay with an 8-μm-pore filter (Corning Costar, NY, USA). Fibroblasts (2×10^4 cells) derived either from the patient or from her unaffected mother and father were resuspended in serum-free medium supplemented or not with 10 ng/ml TGFβ, seeded in the upper chamber, and allowed to migrate for 12 h through the polycarbonate membrane into the bottom well, which was filled with DMEM containing 10% FBS. The cells that did not migrate were removed from the upper surface with a cotton swab. The cells that had migrated in the bottom chamber were fixed in methanol, stained with the Diff-Quik Staining Kit (Medion Diagnostic GmbH, Gräfelfing, Germany), and quantified in 10 non-overlapping fields of 1 mm^2 with a light microscope. Statistical significance was determined using one-way ANOVA followed by Tukey's multiple comparisons test. Data are expressed as means ± SEM from 2 independent experiments performed in triplicate. Analyses were performed with GraphPad Prism software (GraphPad Software, Inc., La Jolla, CA, USA).

2.13. Flow cytometric analysis

Skin fibroblasts of patient and controls were fixed in 80% ethanol for 10 min at −20 °C, resuspended in D-PBS, treated with RNase 20 U (Sigma Aldrich, Germany) for 30 min at 37 °C, and then stained with 10 μg/ml propidium iodide (PI) (Sigma Aldrich, Germany) in PBS. The flow cytometry data were acquired using MoFlo® Astrios™ sorter/analyzer (Beckman Coulter) and analyzed by FlowJo software (TreeStar).

2.14. Autophagy assay

Skin fibroblasts of the patient and controls grown to confluence were harvested and then lysed in 1× D-PBS, 0.025% NP-40, protease- and phospho-inhibitors (Roche, USA). Total lysates were subjected to Western blot analysis as described above. Autophagy was analyzed by detecting the LC3-II (#NB100–2220, Novus, USA) and Beclin-1 (#3738S, Cell Signaling, The Netherlands) protein markers, as previously reported [22]. SDS-PAGE 12% gels were used to clearly separate the LC3-I and LC3-II bands. GAPDH was used as reference protein.

2.15. Statistical analysis

All results are presented as a mean of three independent experiments. Densitometry analysis of immunoblots was performed using the Image J software. Statistical analysis of immunoblotting was performed using unpaired, two-tailed Student's *t*-test (*$p < .05$).

3. Results

3.1. Molecular and in silico findings of the MAP3K7 c.737-7A > G variant

The heterozygous *MAP3K7* c.737-7A > G variant was predicted to generate a new splice acceptor site within intron 7. Sequence chromatograms of RT-PCR products confirmed that the mutant allele creates an additional transcript which includes 6 bases of intron 7 (Fig. 1A). This aberrant transcript was predicted to generate an in-frame insertion of 2 amino acid residues [r.736_737insTTGTAG, p.(Asn245_Gly246insValVal)], which occurs in an evolutionarily conserved region located in the TAK1 kinase and TAB1 binding overlapping domains (Fig. 1B). To predict the pathogenic effect of the novel variant, which localizes between two helices of kinase and the TAB1 binding domains of TAK1 and that is not far from the activation loop, we investigated its structural impact on the TAK1 protein by multiple molecular dynamics (MD) tools. TAK1 wt protein exhibited a stable root-mean-square deviation (RMSD) level at around 0.17 from 131 to 277 ns (ns), before settling at 0.22 nm (nm) after 281 ns till the end of the simulation (Fig. 1C). We recall here that unstable proteins usually exhibit increased RMSD values. In fact, the mutant protein showed higher RMSD levels for almost all simulation timespans (Fig. 1D) and appeared globally less flexible than TAK1 wt, especially when considering the residues making the activation loop (Fig. 1E). The dynamic cross-correlation maps (DCCMs) showed evident changes in the atomic motion dynamics between the wt and mutant proteins. p.(Asn245_Gly246insValVal)-TAK1 caused distant alterations of the protein dynamics, particularly regarding the activation loop, highlighted in red in Fig. 1F and in green in Supp. Movie 1. This portion is the one that contains the amino acids (Thr184, Thr187) responsible for protein autophosphorylation after binding with TAB1.

3.2. The MAP3K7 c.737-7A > G variant affects TAK1 stability, impairs binding with TAB1 and alters signaling downstream of TAK1-TAB1 complex

In order to determine the functional impact of the *MAP3K7* alteration, we first assessed whether the variant alters TAK1 stability by performing quantitative Western blots on protein lysates prepared from cycloheximide-treated HEK293 cells transfected with constructs expressing either wt-TAK1 or p.(Asn245_Gly246insValVal)-TAK1. We detected a weak difference in protein stability between wt and mutant TAK1 protein up to 10 h after cycloheximide treatment. This data may indicate that the pathogenic effect of this allele is partially related to the destabilization of the protein product (Fig. 2A). However, we were not able to appreciate significant differences of endogenous TAK1 amounts between patient's and controls' fibroblasts. The *MAP3K7* c.737-7A > G variant generates an in-frame insertion of 2 amino acid residues in the TAB1 binding domain, which partially overlaps with the TAK1 kinase domain (Fig. 1B). Based on this evidence, we hypothesized that the TAK1 mutated protein loses the ability of interacting with TAB1. To assess our hypothesis, we tested the interaction of TAK1 mutant protein with TAB1 by performing co-immunoprecipitation assays in HEK293 cells transfected with a vector expressing the wt or p.(Asn245_Gly246insValVal)-FLAG-tagged-TAK1. These assays confirmed that the expression of TAK1 mutated protein strongly impairs the formation of the TAK1-TAB1 complex (Fig. 2B). Based on this evidence, we supposed that the impairment of the formation of the TAK1-TAB1 complex affects TAK1 autophosphorylation and activation. Therefore, we first analyzed the endogenous expression level of phosphorylated TAK1 protein by performing Western blot analysis in patient's and controls' fibroblasts. Immunoblot analysis revealed a significant reduction of TAK1 autophosphorylation levels in the patient compared to controls (Fig. 2C). This finding suggests an altered TAK1 activity in the patient, which may result in the dysregulation of the signaling pathways downstream of the TAK1-TAB1 complex, including NF-kB and MAPK.

In order to better explore the functional impact of TAK1 variant, we evaluated its kinase activity by employing a luciferase reporter assay that measures a global readout for transcriptional activation mediated by several MAPK and NF-kB targets. HEK293 cells were transfected with a vector expressing the wt or mutated FLAG-tagged-TAK1 and plasmids containing the MAPK and NF-kB responsive elements (SRE and RE, respectively) upstream of the luciferase reporter gene. We detected a significant 3 and 2.2 fold increase of luciferase signal in cells expressing wt FLAG-tagged TAK1 and MAPK-SRE or NF-kB-RE luciferase reporter plasmids, respectively (Fig. 2D, lane 2 and 5), compared to cells transfected with FLAG-empty vector (Fig. 2D, lane 1 and 3).

Accordingly, we did not observe an increase of luciferase transactivation in cells expressing mutated TAK1 and the reporter plasmids (Fig. 2D, lane 3 and 6). Overall, these data suggest that the TAK1 variant impairs the MAPK-SRE- or NF-kB-RE-mediated luciferase transactivation. Finally, the levels of NF-kB and p-MAPK were quantified in patient's fibroblast lysates by immunoblot analysis that detected a decrease of the NF-kB and p-MAPK levels in patient's cells compared to controls (Fig. 2E and F).

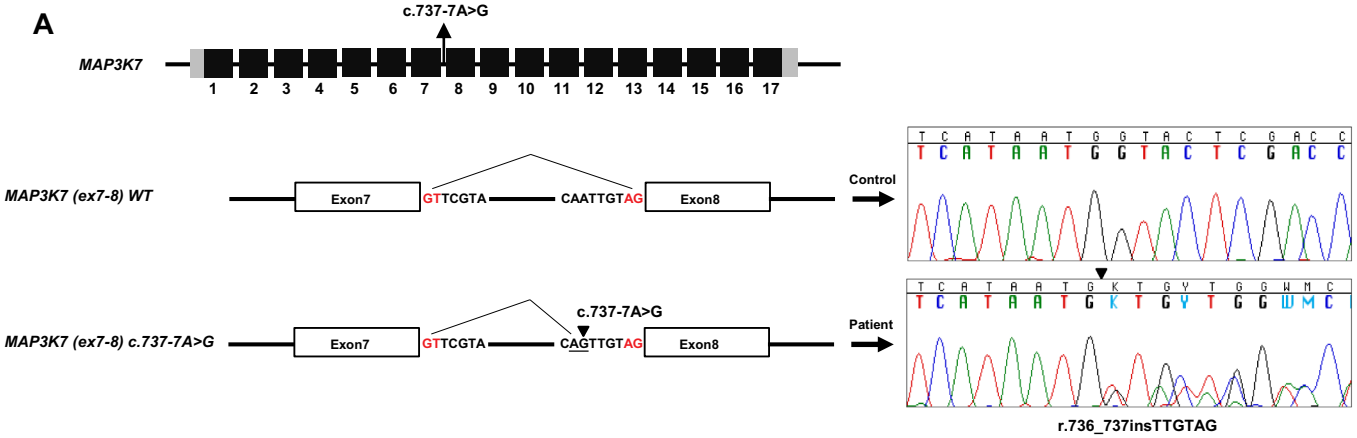

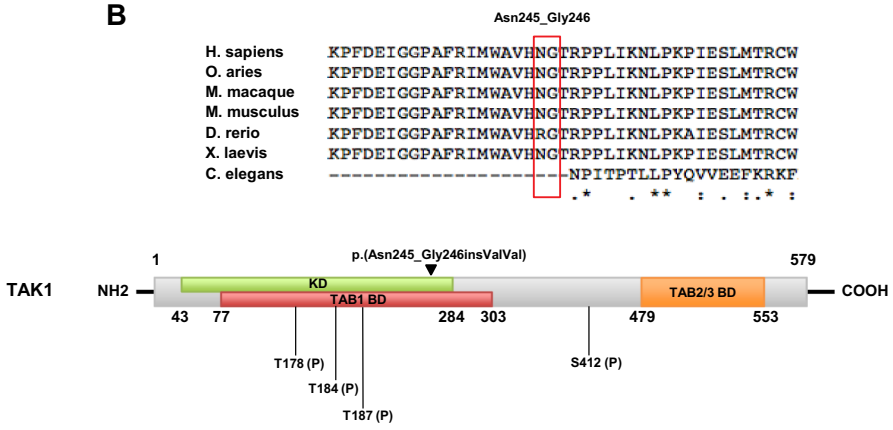

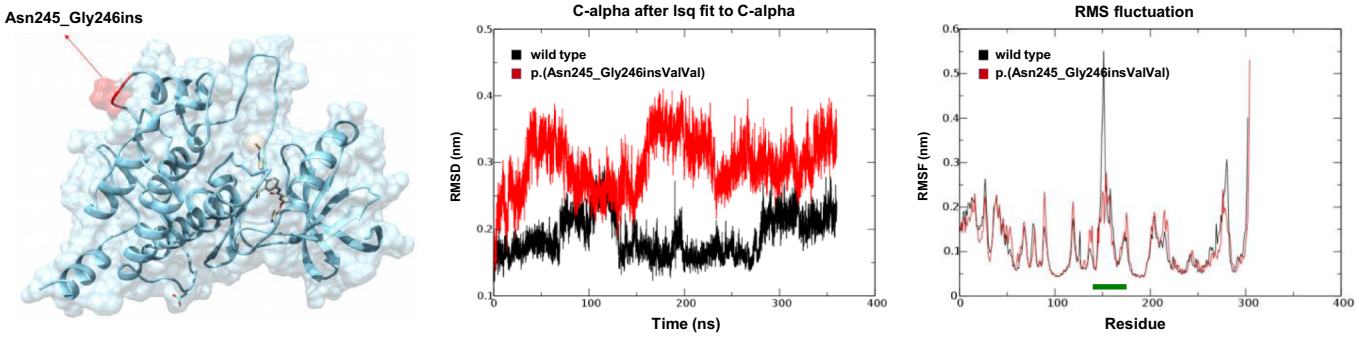

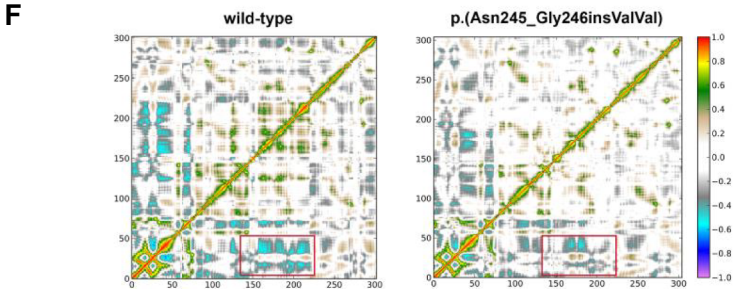

(caption on next page)

Fig. 1. The *MAP3K7* c.737-7A > G variant affects splicing.
(A) Schematic representation of the *TAK1* gene: coding regions are in black, UTR sequences are in grey; introns are not to scale. The variant here described is shown on the gene structure. Schematic representation of normal splicing of the *MAP3K7* region spanning the exons 7 and 8 and aberrant splicing of *MAP3K7* caused by the c.737-7A > G variant. Electropherograms showing sequencing analysis of PCR products amplified with primers targeting exons 7 and 8 of *MAP3K7* cDNA from total RNA extracted from patient and control fibroblasts. Nucleotide sequences are provided. (B) Conservation of the region spanning the residues Asn245 and Gly246 among species and schematic representation of the TAK1 protein. Amino acid positions of each domain are indicated below the structures. KD, kinase domain; TAB1 BD, TAB1 binding domain; TAB2/3 BD, TAB2/3 binding domain. Phosphorylated residues are indicated: T178 (P), T184 (P), T187 (P) and S412 (P). (C) 3D structure of TAK1 protein. p.(Asn245_Gly246insValVal) is highlighted in red; (D) Instantaneous RMSD of all heavy atoms in TAK1 wt (in black) and TAK1 p.(Asn245_Gly246insValVal) mutant (in red); (E) RMSF of residue coordinates in the simulation of TAK1 wt (in black) and TAK1 p.(Asn245_Gly246insValVal) mutant (in red). Localization of the activation loop is marked in green; (F) DCCMs for TAK1 wt (left) and TAK1 p.(Asn245_Gly246insValVal) mutant (right). Red dots identify residues that move in a correlated fashion, whereas blue means that residues move in opposite directions. A red square highlights a groups of residues whose wild-type anti-correlated motions are drastically damped in the mutant. The region includes the activation loop.

3.3. The MAP3K7 c.737-7A > G variant affects the organization of elastic components of the ECM

TGFβ1-induced TAK1 signaling plays a critical role in ECM production, and consequently, in connective tissue homeostasis and function regulation. In this regard, we hypothesized that the impaired TAK1-dependent TGFβ signaling observed in patient's cells may alter ECM organization and component expression in skin fibroblasts which leads to the constellation of clinical features associated to the connective tissue homeostasis deregulation that are displayed by our patient. In order to explore the potential effect of this variant on the ECM organization, we investigated by Immunofluorescence analysis the assembly of COLLI, COLLIII, COLLV, FN, and all FBN isoforms, and the expression of their α2β1 and α5β1 integrin receptors in patient and control fibroblasts. We found that COLLs, FN, and their integrin receptors were organized in a comparable manner both in fibroblasts from the patient and her unaffected parents (Supp. Fig. 1). Regarding FBNs, we found that patient's cells showed an almost complete absence of FBNs fibrils, whereas the control cells organized an abundant and reticular FBNs-ECM (Fig. 3A). These data suggest that the patient's cells, in the presence of impaired TAK1-dependent TGFβ signaling, fail to organize a key ECM component involved in the organization of the elastic network.

3.4. The MAP3K7 c.737-7A > G variant affects the TGFß-mediated organization of the α-SMA cytoskeleton and cell migration

The absence of FBNs fibrils in patient cells suggests a defective adhesion mechanism probably involving integrin receptors different from α5β1 that might affect both cytoskeletal organization and cell migration. To further explore the effect of the *MAP3K7* variant on TAK1-dependent TGFβ signaling, patient's and controls' fibroblasts were analyzed for their capability to organize the cytoskeleton of α-smooth muscle actin (αSMA), a commonly used myofibroblast marker, after treatment with TGFβ. In the absence of serum and without TGFβ, TAK1-mutated fibroblasts did not organize α-SMA stress fibers like control cells and showed impaired adhesion. The treatment with TGFβ induced organization of the α-SMA cytoskeleton in control cells but not in patient's fibroblasts (Fig. 3B).

The failure of cytoskeletal organization was independently corroborated by a migration assay. Specifically, to evaluate whether the *MAP3K7* c.737-7A > G variant affects cell migration in response to TGFβ, a Transwell assay was performed on untreated and TGFβ-treated fibroblasts derived either from the patient or her healthy parents. As shown in Fig. 3C, in the absence of TGFβ, control and patient's cells showed a comparable migratory potential. On the contrary, in the presence of TGFβ, control fibroblasts displayed an enhanced migration (about six- and three-fold increase in CNT1 and CNT2, respectively), whereas patient's cells did not respond to the TGFβ treatment (Fig. 3C). These evidences suggest that the TAK1 mutant protein affects fibroblasts adhesion, migration, and α-SMA cytoskeleton organization.

3.5. The MAP3K7 c.737-7A > G variant affects cell proliferation

The failure of cytoskeletal organization and the reduced protein level of MAPKs in the patient fibroblasts suggest biological alterations in many cellular programs, including cell proliferation, differentiation, motility, and death. In order to address this hypothesis, we evaluated the downstream impact of *MAP3K7* variant on cell cycle progression [27]. We assessed the cell-cycle distribution of patient's and controls' fibroblasts by propidium iodide incorporation and flow cytometry analysis after 24 h of *in vitro* growth and before reaching 90% cell confluency. We discriminated fibroblasts in G0/G1 and S + G2/M phases and found a significant reduction of proliferative S + G2/M cell fraction in the mutant fibroblast compared to wt cells (Fig. 3D and E), supporting the idea that the *MAP3K7* variant impairs the cycling activity of *mutant* cells.

3.6. The MAP3K7 c.737-7A > G variant affects autophagy

It is known that TAK1 signaling pathway induces the expression of the major autophagy-related proteins microtubule-associated protein 1 light chain 3 (LC3) and Beclin-1 (BECN1) that results in autophagy induction [28]. We found a decrease of the LC3-II lipidated form and of Beclin-1 in patient cells compared to controls by immunoblot analysis (Fig. 3F and G). We supported these data by microscopy studies assessing the localization and the signal intensity of endogenous LC3 puncta. In line with Western blot data, we observed a reduction of LC3 intensity signal comparing patient *versus* controls' cells both in basal and stimulation conditions (TGFβ stimulation with or without starvation) (Fig. 3H and I). Altogether, these findings suggest that the *MAP3K7* variant affects the autophagy process.

4. Discussion

In this work, we explored, under multiple perspectives, the pathogenic effects of the *MAP3K7* c.737-7A > G variant, previously identified in a girl with CSCFS and additional signs of soft connective tissue involvement [18]. We showed evidences that the *MAP3K7* c.737-7A > G variant generates a new splice acceptor site, which causes an in-frame insertion of two amino acid residues in the kinase domain. We found that the mutated protein impairs TAK1 ability to bind TAB1 and this, in turn, is demonstrated to alter the activity of TAK1-dependent signaling. We also showed that patients' fibroblasts displayed defective TGFβ-mediated α-SMA cytoskeleton assembly, altered cell proliferation and migration, and impaired autophagy compared to controls. Altogether, these results might explain the coexistence of structural (*i.e.* heart, vertebral, gastrointestinal and facial) and soft connective tissue (*i.e.* articular and skin) findings of the patient, and contribute to predicting the phenotypic spectrum of CSCFS.

In 2016, Le Goff and collaborators [16] discovered *MAP3K7* as the unique gene responsible for CSCFS. in six affected individuals from four unrelated families. In particular, the missense variants c.328G > T, p.(Gly110Cys) and c.721 T > A, p.(Trp241Arg) and the in-frame deletion c.130_135del, p.(Arg44_Gly45del) were found in three sporadic

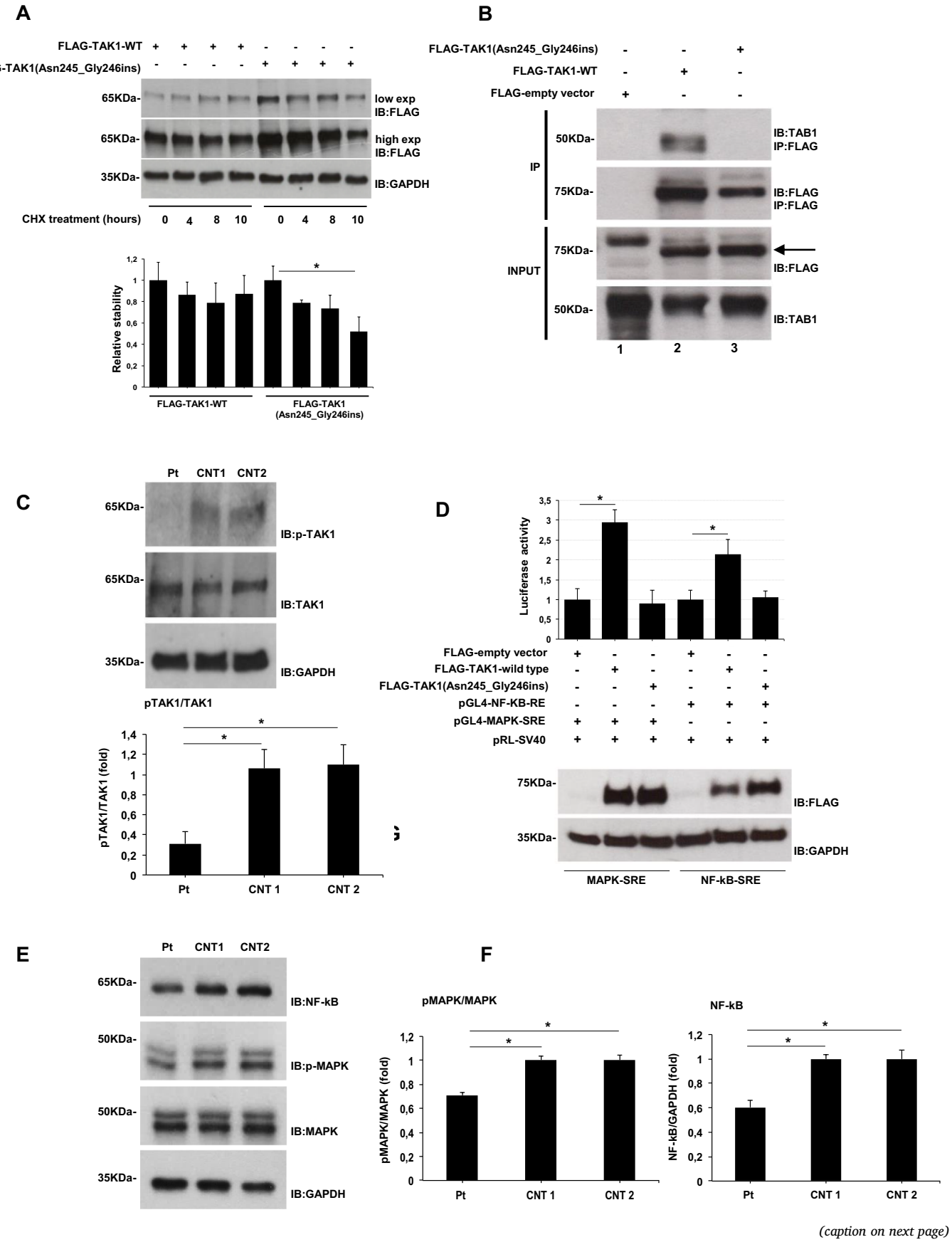

(caption on next page)

Fig. 2. Molecular findings of *MAP3K7* c.737-7A > G variant.
(A) Whole protein lysates of HEK293 cells transfected with vectors encoding FLAG-tagged wt TAK1 or p.(Asn245_Gly246insValVal)-TAK1 and cultured in absence or presence of CHX for 0, 4, 8 and 10 h were separated on 10% SDS - gel and subjected to immunoblotting with anti-FLAG and-GAPDH Abs. Relative quantity of TAK1 p.(Asn245_Gly246insValVal) normalized to wt TAK1 up to 10 h after CHX treatment. Low exp., lower exposition; high exp., higher exposition. (B) HEK293 cells were transfected with vectors encoding FLAG-tagged-TAK1 or FLAG-TAK1 p.(Asn245_Gly246insValVal) or FLAG-empty vectors. Cells were lysed and protein extracts subjected to co-immunoprecipitation using an anti-FLAG Ab. Immunoprecipitated complexes and total lysates were analyzed by immunoblotting using anti-TAB1 and anti-FLAG Abs. (C) Whole protein lysates obtained from skin fibroblasts were separated on 10% SDS-gel and subjected to immunoblotting with indicated antibodies. CNT1 and 2, control individuals; Pt, Patient. Levels of phospho-TAK1/TAK1 were quantified by densitometry using Image J analysis software. Relative phospho-TAK1/TAK1 levels in control cells were set as 1. Graphs show averages calculated on three different experiments and scale bars represent standard errors. Values are expressed as mean ± SEM (*$P < .05$, $n = 3$). (D) Luciferase assays were performed in HEK293 cells co-transfected with a pcDNA3-FLAG-tagged-TAK1 wt or FLAG-tagged- p.(Asn245_Gly246insValVal)-TAK1 and pGL4.32-NF-kB-RE or pGL4.33-MAPK-SRE luciferase reporter plasmids and pRL-SV40 expressing plasmid. Luciferase activities were normalized to the level of *Renilla* luciferase. Whole protein lysates of HEK293 cells transfected with indicated plasmids were separated on 10% SDS-PAGE gel and subjected to immunoblotting with anti-FLAG and –GAPDH Abs. (E) Total lysates were obtained from patient and control skin fibroblasts and separated on 10% SDS-gel and subjected to immunoblotting with indicated Abs. (F) Level of NF-kB and phospho-MAPK/MAPK were quantified by densitometry using Image J analysis software. Relative NF-kB and phospho-MAPK/MAPK levels in control cells were set as 1. Graphs show averages calculated on three different experiments and scale bars represent standard errors. Values are expressed as mean ± SEM (*$P < .05$, $n = 3$).

patients and the c.148_150del, p.(Val50del) variant in a familial case [16]. The variants fall within the kinase domain of TAK1 and patients share growth retardation, dysmorphic facial features, cardiac septal defects with valve dysplasia, upper gut transitory dysfunction and cervical and carpal–tarsal fusions. Functional studies reveal an impaired stimulation of non-canonical TGFβ-1-driven target gene expression that supports a defect in the transcriptional regulation of the MAPK-p38 pathway in fibroblasts obtained from affected individuals [16]. Nevertheless, the limited number of described subjects and the apparent complexity of the molecular mechanisms underlying CSCFS limit our understanding of this disorder.

Differential diagnosis of CSCFS also includes the recently outlined *TAB2* microdeletion syndrome and the phenotype observed in individuals with *TAB2* nonsense variants [19,29,30]. Available data on previously reported individuals with CSCFS and *TAB2* haploinsufficiency indicate some clinical discriminators for these two disorders. In particular, congenital/early-onset gastrointestinal dysmotility is typical of CSCFS, while *TAB2* haploinsufficiency more commonly associates with clinically relevant polyvalvular heart disease. Previously, we demonstrated that TAB2 haploinsufficiency caused by the heterozygous *TAB2* c.1398dup variant results in a decrease of TAK1 autophosphorylation levels that lead to altered activation of more than one downstream signaling pathways [31]. Similar molecular signatures were demonstrated here for the *MAP3K7* c.737-7A > G variant. These findings support the hypothesis of a convergent molecular pathogenesis for *TAB2* haploinsufficiency and selected *MAP3K7* variants, and prompt us to speculate on a recognizable phenotype associated with variants impacting the TAK1-TABs complex and causing dysregulation of TAK1-dependent signaling.

Other work involving animal models reveals a vital role of TAB1 in TAK1 kinase activation and TGFβ signal transduction by forming the TAK1-TAB1 complex. TAB1 interacts constitutively with TAK1 by mediating the autophosphorylation of TAK1 [31] at two threonine residues (Thr184 and Thr187) and a serine residue (Ser192) in the kinase activation loop, and by triggering downstream phosphorylation cascades. Studies in embryonic fibroblasts from *Tab1* and *Tak1*-deficient mice have demonstrated that the TAK1–TAB1 complex plays a pivotal role in embryonic development and morphogenesis [32]. Conditional knockout of *Tak1* in chondrocytes resulted in skeletal defects and severe postnatal growth retardation, and targeted ablation of *Tak1* in osteoblasts showed craniofacial defects. This supports that Tak1 is also essential for maintaining normal pre- and postnatal bone formation [33]. Finally, *in vivo* studies showed that Tak1 also plays a major role in articular cartilage development [34] and cardiac differentiation [35–37]. As TAK1 orchestrates a wide array of cellular functions, it is reasonable to assume that the dysregulation of the TAK1 functions could be associated with pleiotropic clinical features.

Here, we explored the pathological effect of the novel *MAP3K c.737-7A > G* variant. Computational analysis revealed that the TAK1 variant alters the dynamics of the protein that is reflected in the movement of the kinase activation loop which contains the Thr184 and Thr187 amino acids responsible of the autophosphorylation of the protein after binding with TAB1. Our *in vitro* studies revealed that the TAK1 mutated protein impairs the ability to physically bind TAB1. The perturbed TAK1-TAB1 complex destabilizes TAK1, decreases TAK1 phosphorylation levels, and reduces the activity of more than one downstream signaling pathway, such as NF-kB and MAPK. This has relevant consequences on ECM organization, which is crucial in regulating complex cellular behaviors including proliferation, migration, apoptosis, and differentiation. Abnormal composition, structure, or turnover of the ECM characterizes a number of the connective tissue disorders. Interestingly, our patient displayed several signs of soft connective tissue involvement and this prompt us to suppose the ECM disorganization as molecular cause underlying this pathology.

Our hypothesis was supported by accumulating evidences showing that TGFβ-1 induced TAK1 signaling plays a critical role in ECM production. TAK1 is a major upstream signaling molecule in TGFβ-1 induced type I collagen and FN expression through activation of the MAPK kinase (MKK) 3–p38 and MKK4–JNK signaling cascades, respectively [10,38,39]. Conditional *Tak1* gene deletion in mice demonstrates that Tak1 deficiency suppressed interstitial myofibroblast accumulation, collagen deposition, and expression of profibrotic molecules in the kidneys [13]. Our data highlighted that *MAP3K7* patient cells fail to organize the elastic fibers of the ECM. The absence of an organized FBNs-ECM might result in the recruitment of altered integrin settings affecting the cytoskeleton organization. Conversely, the *MAP3K7* variant did not seem to associate with an altered expression of COLLI, COLLIII, COLLV, FN, and the α2β1 and α5β1 integrin receptors. The consequences of the *MAP3K7* c.737-7A > G variant on these ECM components could be slight and, therefore, not appreciable at immunofluorescence analysis. Another explanation is that *MAP3K7* patient cells could organize these ECM proteins through other TAK1-independent signaling pathways.

The documented effect of the *MAP3K7* c.737-7A > G variant on TGFβ-mediated α-SMA cytoskeleton assembly, cell migration and proliferation, and autophagy in patients' cell, in combination with the resulting phenotype, indicates an alteration of fibroblast physiology in CSCFS which could explain some observed clinical features, such as skeletal defects, postnatal growth retardation, and facial features. Moreover, our preliminary data revealed an autophagy defect in *MAP3K7* c.737-7A > G patient's cells, a fact that supports the emerging role for TAK1 as a cellular homeostasis molecule in regulating the autophagy process [40].

In conclusion, we dissected the biological effects of the *MAP3K7 c.737-7A > G* variant and formally demonstrated that CSCFS is well explained by reduced TAK1 autophosphorylation and its multiple downstream cellular consequences. This work contributed to the understanding of the molecular pathogenesis of conditions associated with

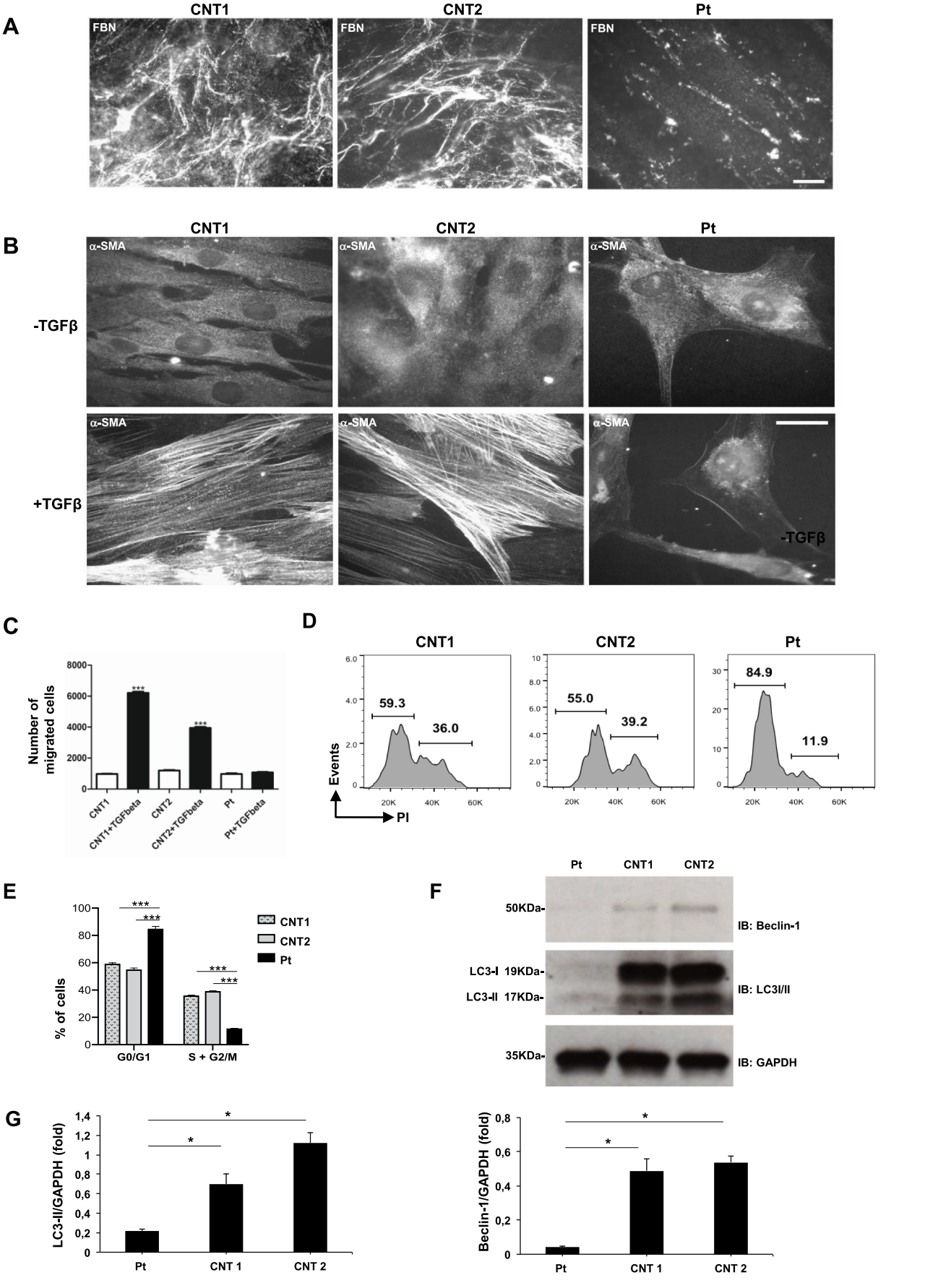

(caption on next page)

Fig. 3. Patient fibroblasts carrying *MAP3K7* c.737-7A > G variant reveal an altered TGFβ-mediated α-SMA cytoskeleton assembly, a partial G0/G1 phase cell-cycle arrest, and an impairment of the autophagic flux.
(A) Immunofluorescence analysis of the FBN isoforms-ECM in fibroblasts from the patient (Pt) and her unaffected mother and father (CNT1 and CNT2, respectively). Scale bar, 10 μm. (B) Immunofluorescence analysis of the α-SMA cytoskeleton in the patient (Pt) and control (CNT1 and CNT2) fibroblasts grown in serum- free medium for 12 h in the absence or presence of 10 ng/ml of TGFβ and immunoreacted with the anti-α-SMA monoclonal Ab. Scale bar: 10 μm. (C) Transwell assay with untreated and TGFβ-treated fibroblasts from the patient (Pt), and her unaffected parents. Data shown represent the means ± SEM from 2 independent experiments performed in triplicate (***$P < .001$ compared to untreated cells). (D) Cell cycle distribution of patient and controls skin fibroblasts was evaluated by flow cytometry after staining with PI. The cells were cultured for 10 days prior to staining. In the plots, the cells in G0/G1 and S + G2/M phases are depicted. Results are representative of multiple replicates. Values are expressed as mean ± SEM (*** $P < .01$, $n = 3$). (E) The bar graph reports the percent of cells in G0/G1 and S + G2/M phases for the wild type and TAK1-mutated fibroblasts, as measured by the reported cell cycle analysis (d). (F) Whole protein lysates of primary skin fibroblasts cell lines from patient and her unaffected mother and father were separated on 12% SDS- gel and subjected to immunoblotting with LC3 and Beclin-1 Abs. The autophagy flux was monitored by the conversion of LC3-I to its lipidated form, LC3-II. GAPDH was used as loading control. (G) Quantification of LC3-II levels. Graph shows averages calculated on two different experiments and scale bars represent standard errors. (* $P < .05$, $n = 2$). (H) Immunofluorescence analyses of LC3 protein in fibroblasts from the proband's unaffected mother and father (CNT1 and CNT2, respectively) and from the patient (Pt) in basal and stimulation conditions (TGFβ stimulation with or without starvation). Scale bars = 10 μm. (I) After acquisition, for all imagies we analyzed the intensity of Alexafluor 568 signal, measuring the relative intensity of pixels representative for each ROI corresponding of a single cell. The graph reports mean ± SEM of LC3 intensity values from 100 cells for each control cell lines compared with 100 cells of proband cell line, and reported in the previous figure. (* $P < .05$, $n = 2$).

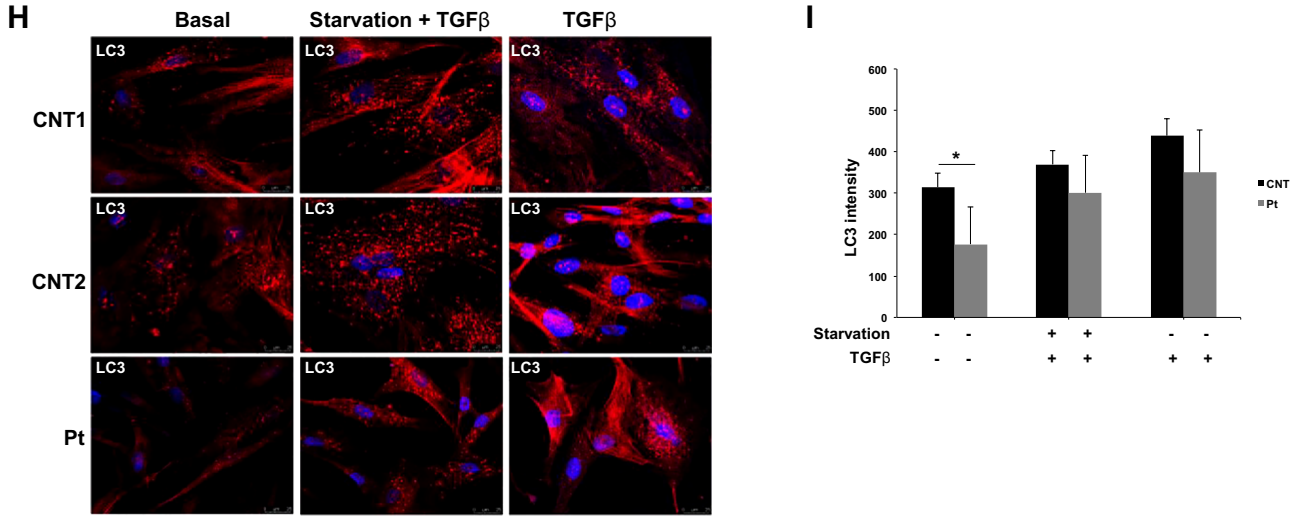

Fig. 3. (*continued*)

alterations of the TAK1-dependent non-canonical TGFβ signaling and, hopefully, to open the path to novel molecular strategies for treating these disorders. Targeting the TGFβ signaling pathway is an emerging therapeutic strategy for many acquired and hereditary disorders. Numerous studies report angiotensin-II as a stimulator of endogenous TGFβ and TAK1 activation in atrial fibroblasts and cardiomyocytes [41,42]. We are confident that further *in vitro* analysis could evaluate the effectiveness of selected molecules restoring the TGFβ signaling, and consequently, to ameliorate some clinical aspects of an increasing number of hereditary conditions, such as CSCFS, which impact this pathway.

Supplementary data to this article can be found online at https://doi.org/10.1016/j.bbadis.2020.165742.

CRediT authorship contribution statement

Lucia Micale: Conceptualization, Data curation, Formal analysis, Funding acquisition, Investigation, Supervision, Validation, Writing - original draft. **Silvia Morlino:** Conceptualization, Data curation, Supervision, Writing - original draft. **Tommaso Biagini:** Software, Data curation, Writing - original draft. **Annalucia Carbone:** Investigation, Methodology, Validation, Writing - review & editing. **Carmela Fusco:** Investigation, Methodology, Validation, Writing - review & editing. **Marco Ritelli:** Investigation, Methodology, Validation, Writing - review & editing. **Vincenzo Giambra:** Investigation, Methodology, Validation, Writing - review & editing. **Nicoletta Zoppi:** Investigation, Methodology, Validation, Writing - review & editing. **Grazia Nardella:** Investigation, Methodology, Validation, Writing - review & editing. **Angelantonio Notarangelo:** Investigation, Methodology, Validation, Writing - review & editing. **Annalisa Schirizzi:** Investigation, Methodology, Validation, Writing - review & editing. **Gianluigi Mazzoccoli:** Writing - review & editing. **Paola Grammatico:** Writing - review & editing. **Emma M. Wade:** Writing - review & editing. **Tommaso Mazza:** Software, Data curation, Writing - original draft. **Marina Colombi:** Conceptualization, Data curation, Formal analysis, Supervision, Validation, Writing - original draft. **Marco Castori:** Conceptualization, Data curation, Formal analysis, Funding acquisition, Supervision, Validation, Writing - original draft.

Acknowledgments

The authors thank the family for their kind availability in sharing the findings within the scientific community. The authors acknowledge Prof. Stephen P. Robertson (University of Otago, Dunedine, New Zealand) for providing pCMV-FLAG-TAK1 plasmid. The authors are also grateful to the Genomic and Genetic Disorder Biobank, member of the Telethon Network of Genetic Biobanks (Telethon Italy grant GTB12001) and the EuroBioBank for providing the specimens. This work was supported by the Ricerca Corrente 2018-2019 Program from the Italian Ministry of Health to LM, GM, TM and MCa and by NVIDIA Corporation and the Amber (California, USA) project to TM. The funders had no role in study design, data collection and analysis, decision

to publish, or preparation of the manuscript. MCo, MR, and NZ thank the Fazzo Cusan family for its generous support.

Declaration of competing interest

The authors declare that they have no known competing financial interests or personal relationships that could have appeared to influence the work reported in this paper.

References

[1] G. Takaesu, S. Kishida, A. Hiyama, et al., TAB2, a novel adaptor protein, mediates activation of TAK1 MAPKKK by linking TAK1 to TRAF6 in the IL-1 signal transduction pathway, Mol. Cell 5 (2000) 649–658.

[2] H. Sakurai, Targeting of TAK1 in inflammatory disorders and cancer, Trends Pharmacol. Sci. 33 (2012) 522–530.

[3] T. Ishitani, G. Takaesu, J. Ninomiya-Tsuji, et al., Role of the TAB2-related protein TAB3 in IL-1 and TNF signaling, EMBO J. 22 (2003) 6277–6288.

[4] A. Adhikari, M. Xu, Z.J. Chen, Ubiquitin-mediated activation of TAK1 and IKK, Oncogene 26 (2007) 3214–3226.

[5] Y. Komatsu, H. Shibuya, N. Takeda, et al., Targeted disruption of the Tab1 gene causes embryonic lethality and defects in cardiovascular and lung morphogenesis, Mech. Dev. 119 (2002) 239–249.

[6] J.K. Mouw, G. Ou, V.M. Weaver, Extracellular matrix assembly: a multiscale deconstruction, Nat Rev Mol Cell Biol 15 (2014) 771–785.

[7] B.Y. Chin, A. Mohsenin, S.X. Li, et al., Stimulation of pro-alpha(1)(I) collagen by TGF-beta(1) in mesangial cells: role of the p38 MAPK pathway, Am J Physiol Renal Physiol 280 (2001) F495–F504.

[8] L. Wang, R. Ma, R.A. Flavell, et al., Requirement of mitogen-activated protein kinase kinase 3 (MKK3) for activation of p38alpha and p38delta MAPK isoforms by TGF-beta 1 in murine mesangial cells, J. Biol. Chem. 277 (2002) 47257–47262.

[9] K. Ono, T. Ohtomo, J. Ninomiya-Tsuji, et al., A dominant negative TAK1 inhibits cellular fibrotic responses induced by TGF-beta, Biochem. Biophys. Res. Commun. 307 (2003) 332–337.

[10] X. Shi-wen, S.K. Parapuram, D. Pala, et al., Requirement of transforming growth factor beta-activated kinase 1 for transforming growth factor beta-induced alpha-smooth muscle actin expression and extracellular matrix contraction in fibroblasts, Arthritis Rheum. 60 (2009) 234–241.

[11] M.E. Choi, Y. Ding, S.I. Kim, TGF-beta signaling via TAK1 pathway: role in kidney fibrosis, Semin. Nephrol. 32 (2012) 244–252.

[12] H.H. Hu, D.Q. Chen, Y.N. Wang, et al., New insights into TGF-beta/Smad signaling in tissue fibrosis, Chem. Biol. Interact. 292 (2018) 76–83.

[13] F.Y. Ma, G.H. Tesch, E. Ozols, et al., TGF-beta1-activated kinase-1 regulates inflammation and fibrosis in the obstructed kidney, Am J Physiol Renal Physiol 300 (2011) F1410–F1421.

[14] Y.G. Zhao, Y. Wang, W. Hao, et al., An essential role for TAK1 in the contact hypersensitivity response, Cell Mol Immunol 8 (2011) 315–324.

[15] M. Neubert, D.A. Ridder, P. Bargiotas, et al., Acute inhibition of TAK1 protects against neuronal death in cerebral ischemia, Cell Death Differ. 18 (2011) 1521–1530.

[16] C. Le Goff, C. Rogers, W. Le Goff, et al., Heterozygous mutations in MAP3K7, encoding TGF-beta-activated kinase 1, cause cardiospondylocarpofacial syndrome, Am. J. Hum. Genet. 99 (2016) 407–413.

[17] E.M. Wade, Z.A. Jenkins, P.B. Daniel, et al., Autosomal dominant frontometaphyseal dysplasia: delineation of the clinical phenotype, Am. J. Med. Genet. A 173 (2017) 1739–1746.

[18] S. Morlino, M. Castori, C. Dordoni, et al., A novel MAP3K7 splice mutation causes cardiospondylocarpofacial syndrome with features of hereditary connective tissue disorder, Eur. J. Hum. Genet. 26 (2018) 582–586.

[19] M. Ritelli, S. Morlino, E. Giacopuzzi, et al., A recognizable systemic connective tissue disorder with polyvalvular heart dystrophy and dysmorphism associated with TAB2 mutations, Clin. Genet. 93 (2018) 126–133.

[20] T. Biagini, G. Chillemi, G. Mazzoccoli, et al., Molecular dynamics recipes for genome research, Brief. Bioinform. 19 (2018) 853–862.

[21] E.M. Wade, P.B. Daniel, Z.A. Jenkins, et al., Mutations in MAP3K7 that Alter the activity of the TAK1 signaling complex cause frontometaphyseal dysplasia, Am. J. Hum. Genet. 99 (2016) 392–406.

[22] P. Palumbo, A. Petracca, R. Maggi, et al., A novel dominant-negative FGFR1 variant causes Hartsfield syndrome by deregulating RAS/ERK1/2 pathway, Eur. J. Hum. Genet. 27 (2019) 1113–1120.

[23] N. Zoppi, R. Gardella, A. De Paepe, et al., Human fibroblasts with mutations in COL5A1 and COL3A1 genes do not organize collagens and fibronectin in the extracellular matrix, down-regulate alpha2beta1 integrin, and recruit alphavbeta3 instead of alpha5beta1 integrin, J. Biol. Chem. 279 (2004) 18157–18168.

[24] N. Chiarelli, G. Carini, N. Zoppi, et al., Transcriptome-wide expression profiling in skin fibroblasts of patients with joint hypermobility syndrome/Ehlers-Danlos syndrome hypermobility type, PLoS One 11 (2016) e0161347.

[25] N. Zoppi, S. Barlati, M. Colombi, FAK-independent alphavbeta3 integrin-EGFR complexes rescue from anoikis matrix-defective fibroblasts, Biochim. Biophys. Acta 2008 (1783) 1177–1188.

[26] N. Zoppi, N. Chiarelli, S. Binetti, et al., Dermal fibroblast-to-myofibroblast transition sustained by alphavss3 integrin-ILK-Snail1/Slug signaling is a common feature for hypermobile Ehlers-Danlos syndrome and hypermobility spectrum disorders, Biochim. Biophys. Acta Mol. Basis Dis. 2018 (1864) 1010–1023.

[27] E. Omori, K. Matsumoto, S. Zhu, et al., Ablation of TAK1 upregulates reactive oxygen species and selectively kills tumor cells, Cancer Res. 70 (2010) 8417–8425.

[28] Y. Ding, J.K. Kim, S.I. Kim, et al., TGF-{beta}1 protects against mesangial cell apoptosis via induction of autophagy, J. Biol. Chem. 285 (2010) 37909–37919.

[29] Cheng A, Dinulos MBP, Neufeld-Kaiser W et al. 6q25.1 (TAB2) microdeletion syndrome: Congenital heart defects and cardiomyopathy. Am J Med Genet A 2017.

[30] Morlino S, Carbone A, Ritelli M et al. TAB2 c.1398dup variant leads to haploinsufficiency and impairs extracellular matrix homeostasis. Hum Mutat 2019.

[31] L. Dai, C. Aye Thu, X.Y. Liu, et al., TAK1, more than just innate immunity, IUBMB Life 64 (2012) 825–834.

[32] L.M. Gunnell, J.H. Jonason, A.E. Loiselle, et al., TAK1 regulates cartilage and joint development via the MAPK and BMP signaling pathways, J. Bone Miner. Res. 25 (2010) 1784–1797.

[33] W. Liu, B.L. Chang, S. Cramer, et al., Deletion of a small consensus region at 6q15, including the MAP3K7 gene, is significantly associated with high-grade prostate cancers, Clin. Cancer Res. 13 (2007) 5028–5033.

[34] M.B. Greenblatt, J.H. Shim, L.H. Glimcher, TAK1 mediates BMP signaling in cartilage, Ann. N. Y. Acad. Sci. 1192 (2010) 385–390.

[35] K. Brown, S. Legros, J. Artus, et al., A comparative analysis of extra-embryonic endoderm cell lines, PLoS One 5 (2010) e12016.

[36] M. Xie, D. Zhang, J.R. Dyck, et al., A pivotal role for endogenous TGF-beta-activated kinase-1 in the LKB1/AMP-activated protein kinase energy-sensor pathway, Proc. Natl. Acad. Sci. U. S. A. 103 (2006) 17378–17383.

[37] J.L. Jadrich, M.B. O'Connor, E. Coucouvanis, The TGF beta activated kinase TAK1 regulates vascular development in vivo, Development 133 (2006) 1529–1541.

[38] S.I. Kim, J.H. Kwak, M. Zachariah, et al., TGF-beta-activated kinase 1 and TAK1-binding protein 1 cooperate to mediate TGF-beta1-induced MKK3-p38 MAPK activation and stimulation of type I collagen, Am J Physiol Renal Physiol 292 (2007) F1471–F1478.

[39] B.A. Hocevar, C. Prunier, P.H. Howe, Disabled-2 (Dab2) mediates transforming growth factor beta (TGFbeta)-stimulated fibronectin synthesis through TGFbeta-activated kinase 1 and activation of the JNK pathway, J. Biol. Chem. 280 (2005) 25920–25927.

[40] G. Herrero-Martin, M. Hoyer-Hansen, C. Garcia-Garcia, et al., TAK1 activates AMPK-dependent cytoprotective autophagy in TRAIL-treated epithelial cells, EMBO J. 28 (2009) 677–685.

[41] J. Gu, X. Liu, Q.X. Wang, et al., Angiotensin II increases CTGF expression via MAPKs/TGF-β1/TRAF6 pathway in atrial fibroblasts, Exp. Cell Res. 318 (2012) 2105–2115.

[42] S.J. Watkins, G.M. Borthwick, R. Oakenfull, et al., Angiotensin II-induced cardiomyocyte hypertrophy in vitro is TAK1-dependent and Smad2/3-independent, Hypertens. Res. 35 (2012) 393–398.